THE JOURNAL OF PHYSICAL CHEMISTRY A

 VOLUME 113, NUMBER 14, APRIL 9, 2009

ARTICLES

Photodissociation Dynamics of Alkyl Nitrites at 266 and 355 nm: The OH Product Channel

Xian-Fang Yue, Ju-Long Sun, Hong-Ming Yin, Qiang Wei, and Ke-Li Han*

State Key Laboratory of Molecular Reaction Dynamics, Dalian Institute of Chemical Physics, Chinese Academy of Sciences, Dalian 116023, China

Received: December 06, 2008; Revised Manuscript Received: February 11, 2009

Photodissociation of methyl nitrite and *n*-butyl nitrite at 266 and 355 nm has been investigated in the gas phase at room temperature. OH photoproducts were observed, and their internal state distributions were measured by the one-photon laser-induced fluorescence (LIF) technique. It was found that the nascent OH from the 266 nm photolysis of methyl nitrite was vibrationally cold, and its rotational state distribution conformed to a Boltzmann behavior with a rotational temperature of $T_{rot} = 2200 \pm 150$ K. In contrast, the nascent OH from the 266 nm photolysis of *n*-butyl nitrite was found to be vibrationally excited, and the measured relative population of $v'' = 0$:1 was 0.78: 0.22. The rotational state distribution of the OH $v'' = 1$ state conformed to Boltzmann behavior, with a rotational temperature of $T_{rot} = 1462 \pm 120$ K. However, a simple Boltzmann distribution was not found for the OH $v'' = 0$ state. In the photolysis of *n*-butyl nitrite at 355 nm, the OH fragment was found to be vibrationally cold and its rotational state distribution showed non-Boltzmann behavior. A photodissociation mechanism involving an intramolecular hydrogen atom transfer process is proposed for the OH product pathway for methyl nitrite, which has been compared with the potential energy surfaces obtained from density functional theory (DFT) calculations. A photodissociation mechanism of *n*-butyl nitrite is also proposed for the OH product pathway, which differs from that of methyl nitrite due to the effects of the different alkoxy substituents.

I. Introduction

Photodissociation of polyatomic molecules is one of the major chemical processes. Its study is fundamental for a better understanding of the nature of elementary reactions, i.e., the breaking and forming of chemical bonds.[1−3] Alkyl nitrites, generally denoted as RONO, where R represents an alkyl moiety (e.g., methyl, ethyl, isopropyl, etc.), are excellent candidates for photodissociation investigations since their dissociation is fast (< rotational period) and product quantum states carry memory of the initial excitation.[4] The UV absorption spectra of RONO species are very similar and consist of two excitation bands. The first weak absorption band, in the range 300−400 nm, is the S_1 ($n\pi^*$) ← S_0 transition, corresponding to the excitation of one electron of the lone pair on oxygen to the π^* antibonding orbital. The second strong absorption band is due to the S_2 ($\pi\pi^*$) ← S_0 transition centered at about 220 nm.[5] In both absorption bands, the primary photodissociation process is cleavage of the weak RO−NO bond (∼41 kcal/mol)[6] to yield the alkoxy radical and nitric oxide.

$$\mathrm{RONO}(S_0) + h\nu \rightarrow \mathrm{RO}(\mathrm{A\ or\ X}) + \mathrm{NO}(X^2\Pi) \qquad (1)$$

Most of the past studies on the reaction according to eq 1 have been focused on methyl nitrite (CH_3ONO),[5,7−30] ethyl nitrite (CH_3CH_2ONO),[28,31] and *tert*-butyl nitrite ($(CH_3)_3CONO$).[4,10,16,24,29,30,32−37] Lahmani et al.[7−9] investigated the photodissociation of CH_3ONO between wavelengths of 364 and 318 nm by probing the NO

* To whom correspondence should be addressed. E-mail: klhan@dicp.ac.cn.

10.1021/jp810731d CCC: $40.75
Published on Web 03/13/2009

product state distributions by means of the two-photon LIF technique. Pfab and co-workers[10−12] reported on the photolysis of jet-cooled CH_3ONO at 387, 380, and 355 nm. Schwartz-Lavi et al.[32,33] studied the photodissociation of $(CH_3)_3CONO$ at 365.8 and 351.8 nm. They measured the rotational alignment, $\boldsymbol{\mu}$, $\mathbf{v}$, and $\mathbf{J}$ vector correlations, energy disposals, and internal state distributions (vibration, rotation, Λ-doublet, and spin−orbit components) of the nascent NO fragments by single-photon LIF combined with polarization and sub-Doppler spectroscopy.[32,33] All of these authors determined highly non-Boltzmann rotational state distributions, small vibrationally excited and inverted state distributions, and various vectorial behaviors of the nascent NO fragments, from which it was concluded that the S_1 state is a short-lived predissociative state.[11,12,32,33] Mestdagh et al.[29] determined the dissociation times (about 125 fs) of the S_1 states of methyl nitrite, *n*- and *tert*-butyl nitrite, and isoamyl nitrite by the time-resolved LIF technique.

In contrast to the detailed studies of the S_1 state of alkyl nitrites, few reports have been concerned with the second absorption band. Winniczek et al.[25] studied the photodissociation of the S_2 state of CH_3ONO at 223−227 nm by the resonantly enhanced multiphoton ionization (REMPI) photoelectron spectroscopy technique. Yin et al.[26] measured the internal state distributions and alignment effects of the NO fragments from the 266 nm photolysis of methyl nitrite by the polarized one-photon LIF technique. Schwartz-Lavi and Rosenwaks[33] investigated the detailed scalar and vectorial properties of the NO photoproducts from the 250 nm photodissociation of $(CH_3)_3CONO$. All of these authors determined highly inverted and Gaussian-like rotational state distributions, dominant ground vibrational ($v'' = 0$) state populations, and negative alignment ($A_0^{(2)}$) values of the nascent NO products, from which it was concluded that the S_2 surface is strongly repulsive and promotes rapid direct dissociation.[26,33] Farmamara et al.[5] determined the lifetime of the S_2 state of CH_3ONO as lying in the range 25(±15) fs using the femtosecond pump−probe technique. Huber's group[13,27,30,35] investigated the translational energy distributions of the RO and NO fragments derived from the photolysis of methyl nitrite, ethyl nitrite, isopropyl nitrite, and *tert*-butyl nitrite in both the S_1 and S_2 states, and their results were consistent with the conclusions mentioned above. On the other hand, Finke et al.[4] observed highly inverted vibrational state distributions and less excited rotational state distributions of the NO fragments derived from the 193 nm photolysis of $(CH_3)_3CONO$, which were very different from the results obtained by Schwartz-Lavi and Rosenwaks[33] at 250 nm. They proposed the existence of an additional "vibrationally adiabatic" dissociation potential energy surface (PES) in the short-wavelength region.[4] Castle et al.[34] also found the inverted vibrational state distributions of the NO fragments derived from the photolysis of *tert*-butyl nitrite at short wavelengths near 200 nm. Unfortunately, there have been no corresponding theoretical calculations on the PES suggested by Finke et al.[4]

Other photodissociation pathways for alkyl nitrite molecules have rarely been reported in the literature. In a previous Letter,[38] we presented preliminary results concerning the OH product channel from the 266 nm photolysis of CH_3ONO. The origin of the OH fragment was initially assigned to the following decay channel:

$$CH_3ONO + h\nu(266\ \text{nm}) \rightarrow NO(X^2\Pi) + CH_3O(X^2E) \quad (2)$$

$$CH_3O(X^2E) \rightarrow CH_2OH(^2A) \rightarrow CH_2(^3B1) + OH(X^2\Pi) \quad (3)$$

In the present work, we propose a hydrogen-transfer photodissociation mechanism for the OH product pathway for CH_3ONO, which has been compared with the results of DFT calculations. In addition, we have investigated the photodissociation of gaseous $CH_3(CH_2)_3ONO$ at 266 and 355 nm. The OH photoproducts have been observed and their internal state distributions have been measured with the one-photon LIF technique. A dissociation mechanism corresponding to the OH product channel for $CH_3(CH_2)_3ONO$ is also proposed.

II. Experimental Section

The experimental apparatus used in the present study has been described in detail elsewhere.[26,38] Briefly, the second-harmonic output (532 nm) of an Nd:YAG laser (Spectra- Physics, GCR-170, 10 Hz) was used to pump a tunable dye laser (Lumonics HD-500) operating with DCM dye. The output of the dye laser was again frequency-doubled through a Harmonic Generator (Lumonics, HT-1000) and used for the probe laser beam. The residual part of the 1064 nm output of the Nd:YAG laser was converted to 266 (4−5 ns duration) or 355 nm (5−6 ns duration) by KD*P crystals and provided the photolysis laser beam. These two laser beams were collinearly counterpropagated and softly focused on the center of the photolysis cell by respective 70 cm focal length lenses. The focused spot sizes of the photolysis laser beam and probe laser beam were ∼2 and ∼3 mm, respectively, at the center of the photolysis cell. The photolysis laser pulse energy used in the experiments was reduced to less than 1.2 mJ to ensure that OH formation from multiphoton processes was negligible. The probe laser pulse energy was reduced to ∼0.1 mJ. The probe laser beam was optically delayed with respect to the photolysis beam by ∼15 ns. This delay period was sufficient to separate the two laser beams, and was short enough to make collision effects negligible under the pressure (typically 70 mTorr) used in the experiments.

The resulting fluorescence was collected by a lens with a focal length of 50 mm (diameter: 50 mm) and detected by a photomultiplier tube (PMT, Hamamatsu CR161). A suitable band-pass filter was placed in front of the PMT to cut off scattering from the photolysis laser. The signal from the PMT was then gate-integrated by a Boxcar (SRS, SR250), A/D converted by means of a homemade interface, and stored in a personal computer with use of a data-taking program. In the experiments, the linearity of the LIF intensity with respect to variations in the power of each of the lasers and the pressure within the photolysis cell was carefully checked to avoid saturation effects. Each LIF spectrum was recorded at least three times to ensure a true signal.

All experiments were conducted on "slow flows" so that photolysis products did not build up during successive 10 Hz pulses. *n*-Butyl nitrite (95%) was purchased from Acros Organics and was used without further purification. *n*-Butyl nitrite vapor was formed by passing ultrapure He at a pressure of 760 Torr through a reservoir filled with the sample at 298 K. The sample/He mixture was continuously expanded into the center of the photolysis cell through a 0.4 mm internal diameter tube. This gas mixture was then coincident with the focused photolysis and probe laser beams at the center of the photolysis cell. The pressure within the photolysis cell was monitored by means of a capacitance manometer and maintained at ∼70 mTorr during the data acquisition.

The preparation of methyl nitrite was described in our previous Letter.[39] Nitrous acid (HONO) was prepared by the dropwise addition of dilute sulfuric acid (10% by volume) to a dilute solution of sodium nitrite (0.1 M). He carrier gas at a pressure of 760 Torr entered the HONO generator through a frit at the bottom and bubbled through the liquid sample. The HONO/He gas mixture passed through a 25 cm long glass drying tube filled with $CaCl_2$ as desiccant, and then expanded into the center of the photolysis cell. The pressure within the photolysis cell was again maintained at ∼70 mTorr during the data acquisition.

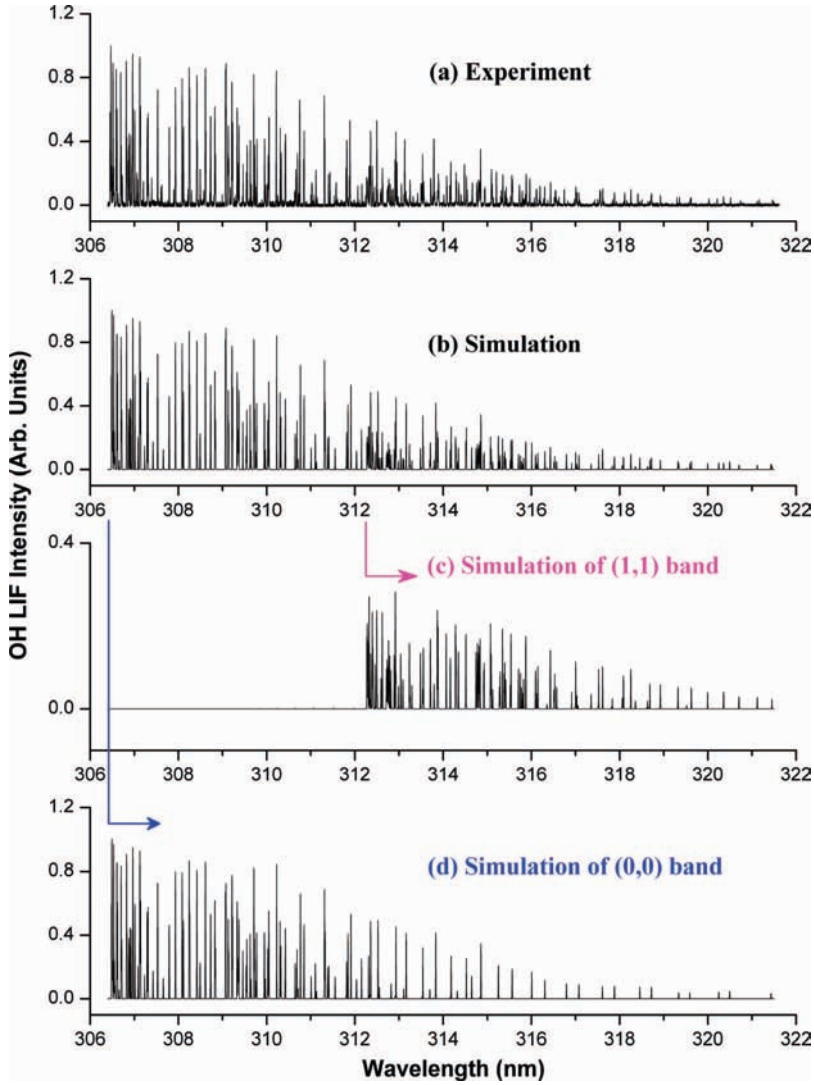

Figure 1. A portion of the $A^2\Sigma^+(v'=0) \leftarrow X^2\Pi(v''=0)$ and $A^2\Sigma^+(v'=1) \leftarrow X^2\Pi(v''=1)$ bands of the one-photon excited LIF spectra of the nascent OH from the photolysis of $CH_3(CH_2)_3ONO$ at 266 nm: (a) experiment; (b) simulation; (c) (1, 1) band simulation; and (d) (0, 0) band simulation.

III. Results and Discussion

A. LIF Spectra of OH from the Photolysis of $CH_3(CH_2)_3ONO$ and CH_3ONO. The LIF spectra of nascent $OH(X^2\Pi)$ fragments from the photolysis of $CH_3(CH_2)_3ONO$ at 266 nm were recorded by scanning the OH $A^2\Sigma^+(v'=0) \leftarrow X^2\Pi(v''=0, 1)$ transitions in the range 306−322 nm. No LIF signals of the vibrationally excited $OH(X^2\Pi, v''=2)$ were observed, even when using higher photolysis laser power and increasing the probe laser intensity. It is known that the ground electronic state ($X^2\Pi$) of OH is split into two spin−orbit components $F_1(^2\Pi_{3/2})$ and $F_2(^2\Pi_{1/2})$; each of them is split again into two Λ-doublet states $\Pi^+(A')$ and $\Pi^-(A'')$. Consequently, 12 sub-branches are involved in the OH $A^2\Sigma^+ \leftarrow X^2\Pi$ transition. Limited by the experimental resolution, only eight sub-branches could be resolved. On the other hand, the bands of OH(0, 0) and OH(1, 1) are overlapped, especially at wavelengths longer than 312.27 nm (band head of R_{11} sub-branch). To precisely assign the J″ levels of each vibrational state of OH populated in the dissociation process, it is necessary to compare the experimental spectra with the simulated ones calculated from the known spectroscopic constants. Figure 1 depicts the experimental and simulated spectra of the nascent OH (0, 0) and (1, 1) bands from the photodissociation of *n*-butyl nitrite at 266 nm. To compare the contributions to the overlapped spectra (Figure 1a) from the respective (0, 0) and (1, 1) bands, panels c and d of Figure 1 display the simulated (1, 1) and (0, 0) bands, respectively. Clearly, the LIF intensity of the (0, 0) band is much stronger than that of the (1, 1) band.

For the photodissociations of $CH_3(CH_2)_3ONO$ at 355 nm and CH_3ONO at 266 nm, the nascent OH fragments were found to be vibrationally cold ($v'' = 0$). The LIF spectra of the $A^2\Sigma^+(v'=0) \leftarrow X^2\Pi(v''=0)$ transitions were recorded in the region 306−316 nm. The experimental and simulated spectra of the OH (0, 0) band from the 355 nm photolysis of $CH_3(CH_2)_3ONO$ and the 266 nm photolysis of CH_3ONO are not illustrated here. For the photodissociation of CH_3ONO at 355 nm, the LIF spectrum of the OH (0, 0) band was superimposed on the LIF spectrum of the CH_3O $A^2A_1(v_3'=0) \leftarrow X^2E(v_3''=0)$ transitions[39] in the range 306−316 nm, which resulted in a low signal-to-noise ratio of the LIF spectrum of the OH (0, 0) band. We have been unable to obtain good results for the photodissociation of CH_3ONO at 355 nm. Therefore, these results are not included in the present work. Since the one-photon excitation process $A^2\Sigma^+ \leftarrow X^2\Pi$ is easily characterized, scalar properties of the nascent OH product derived from the photodissociation can be obtained from the LIF spectra. A detailed analysis of the internal state distributions of the OH fragments is presented in the following.

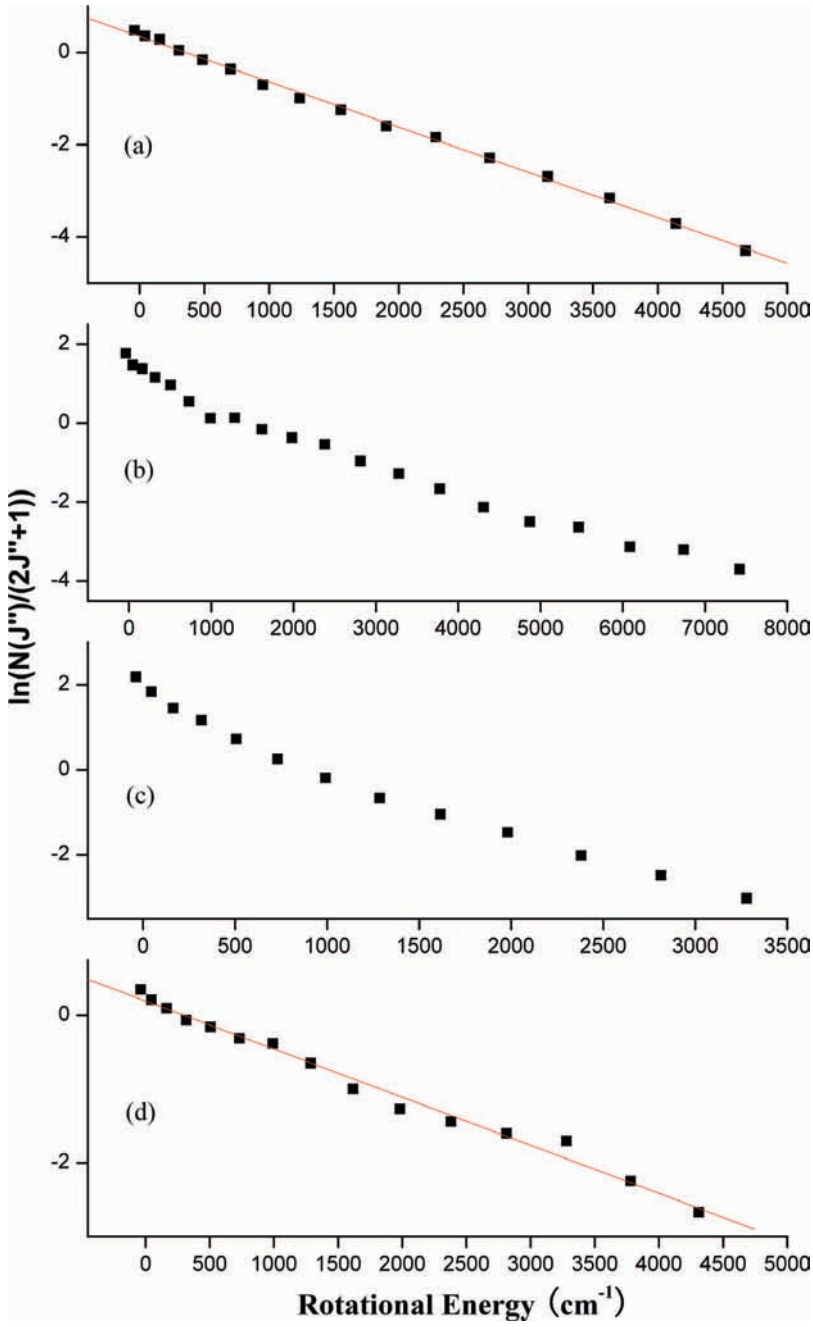

Figure 2. Boltzmann plots of the rotational state distributions of the following: (a) OH($X^2\Pi_{3/2}(v''=1)$) from the photolysis of $CH_3(CH_2)_3ONO$ at 266 nm; (b) OH($X^2\Pi_{3/2}(v''=0)$) from the photolysis of $CH_3(CH_2)_3ONO$ at 266 nm; (c) OH($X^2\Pi_{3/2}(v''=0)$) from the photolysis of $CH_3(CH_2)_3ONO$ at 355 nm; and (d) OH($X^2\Pi_{3/2}(v''=0)$) from the photolysis of CH_3ONO at 266 nm. The solid lines in panels a and d are the best linear fits to the experimental data at Boltzmann temperatures of $T_{rot} = 1462$ and 2200 K, respectively.

B. Rotational and Vibrational State Distributions and Energies. The OH transitions were labeled following Hund's case (a).[40] The P, Q, and R branches relate to the cases of $\Delta J = -1$, 0, and 1, respectively. The rotational state population $N(J'', v'')$ of each vibrational state in the ground electronic state can be obtained from the spectral intensities of the P, Q, and R branches. The relationship between the intensity (I_F) and the population is expressed as:

$$I_F \propto \frac{N(J'', v'')q_{v'v''}S_{J'J''}f(\nu, \nu_0)}{(2J'' + 1)} \quad (4)$$

where $q_{v'v''}$ are the known Franck−Condon factors for the OH A−X transition,[41] $S_{J'J''}$ are the line strengths for the OH A−X one-photon rotational transitions,[42] and $f(\nu,\nu_0) = \rho(\nu_0)\exp(-a(\nu - \nu_0)^2)$ is the laser intensity function. To compare the measurement of each rotational level, spectral intensities of the observed LIF rotational lines were normalized with respect to the pressure of the sample in the photolysis cell as well as the probe and photolysis laser energies. On the basis of these normalized intensities, the rotational state populations were calculated from eq 4. Figure 2 shows typical Boltzmann plots of the normalized population distributions of the nascent OH($X,^2\Pi_{3/2}$) derived from the 266 and 355 nm photolyses of $CH_3(CH_2)_3ONO$ and the 266 nm photolysis of CH_3ONO. The solid lines in panels a and d of Figure 2 are the best linear fits to the experimental data. The vibrationally excited state ($v'' = 1$) of OH($X,^2\Pi$) was exclusively

TABLE 1: Internal Energy Content of the OH($X^2\Pi$) from the Photodissociation of $CH_3(CH_2)_3ONO$, CH_3ONO, and HONO at 266 or 355 nm[a]

	λ_{ph}	v''	$P_{v''}$	E^v_{rot}	$E^v_{rot}P_{v''}$	E_{rot}	E^v_{vib}	$E^v_{vib}P_{v''}$	E_{vib}
$CH_3(CH_2)_3ONO$	266	0	0.78	1157	1012	1119	1848	1441	2633
		1	0.22	986	217		5417	1192	
	355					986			
CH_3ONO	266					1221			

[a] All energies are in cm^{-1}.

found in the photolysis of $CH_3(CH_2)_3ONO$ at 266 nm. Its rotational state distribution conformed to a Boltzmann behavior, and the rotational Boltzmann temperature was calculated from the slope of the solid line (Figure 2a) as $T_{rot} = 1462 \pm 120$ K. As shown in Figure 2b, the rotational state distribution of the OH $v'' = 0$ state derived from the photolysis of $CH_3(CH_2)_3ONO$ at 266 nm does not display single Boltzmann behavior, and hence it cannot be described by a simple rotational temperature. In the photolysis of $CH_3(CH_2)_3ONO$ at 355 nm, the rotational state distribution of the OH $v'' = 0$ state is non-Boltzmann (Figure 2c). Its maximum rotational population was monitored up to $J'' = 13.5$, which was smaller than that ($J'' = 20.5$) of the OH $v'' = 0$ state derived from the 266 nm photolysis of $CH_3(CH_2)_3ONO$ (Figure 2b).

For the 266 nm photodissociation of CH_3ONO, the nascent OH fragment was found to be vibrationally cold. Its rotational state distribution conformed to Boltzmann behavior with a rotational temperature of $T_{rot} = 2200 \pm 150$ K. The maximum rotational population was monitored up to $J'' = 15.5$ (Figure 2d), which was again smaller than that ($J'' = 20.5$) of the OH $v'' = 0$ state from the photolysis of $CH_3(CH_2)_3ONO$ at 266 nm. Clearly, the vibrational and rotational state distributions of the OH from the 266 nm photodissociation of CH_3ONO are very different from those of the OH from the 266 nm photodissociation of $CH_3(CH_2)_3ONO$. This indicates that the photolysis mechanisms of these two molecules at 266 nm must be different, which primarily results from the effects of the different alkoxyl substituents.

The rotational energy content $E^v_{rot}$of each vibrational level was calculated by summing the energyE^J_{rot}over each J'' and multiplying by the normalized relative population. The average rotational and vibrational energies E_{rot} and E_{vib}were obtained by summing the rotational and vibrational energy content (E^v_{rot}andE^v_{vib}) and multiplying by the normalized relative population $P_{v''}$. Table 1 lists these energy contents and the relative populations of the nascent OH from the photodissociations of $CH_3(CH_2)_3ONO$ and CH_3ONO. As shown in Table 1, the ground vibrational state of OH was found to be most populated following the 266 nm photolysis of $CH_3(CH_2)_3ONO$. The measured relative population of $v'' = 0$:1 was 0.78:0.22. In the $CH_3(CH_2)_3ONO$ photodissociation at 355 nm and the CH_3ONO photodissociation at 266 nm, the OH fragments were vibrationally cold. Their average rotational energies are listed in Table 1.

C. Spin−Orbit State Distributions. The two spin−orbit states $F_1(^2\Pi_{3/2})$ and $F_2(^2\Pi_{1/2})$ arise from two possible spin−orbit couplings of the total rotational angular momentum **K** and the spin angular momentum **S**, yielding the total angular momentum $\mathbf{J} = \mathbf{K} + \mathbf{S}$, where $\mathbf{J} = \mathbf{K} + {}^1/_2$ for F_1 and $\mathbf{J} = \mathbf{K} - {}^1/_2$ for F_2.[26] Ratios of the populations of $^2\Pi_{3/2}/^2\Pi_{1/2}$ versus the rotational quantum number J are plotted in Figure 3: panels a and b in Figure 3 relate to the nascent OH from the $CH_3(CH_2)_3ONO$ photolyses at 266 and 355 nm, respectively; Figure 3c relates to the nascent OH from the CH_3ONO photolysis at 266 nm. Clearly, the $^2\Pi_{3/2}$ spin−orbit level is slightly preferentially populated in each vibrational state of the OH from the aforementioned photodissociations. It is interesting to note that since the F_1 state lies at a lower energy spin−orbit state, the rotational state energy with the rotational quantum number J in the F_1 state is lower than that in the F_2 state. Therefore, the rotational state distributions are expected to be primarily populated in the J values of the OH fragment in the F_1 state compared to that in the F_2 state. This energetic difference of the two spin−orbit states could be partly responsible for the ratios of F_1/F_2 seen in Figure 3. Preferential population of the F_1 spin−orbit state has also been found for OH photofragments produced by photodissociations of HONO,[43] HCOOH,[44] acetylacetone,[45] and enolic-acetylacetone.[46]

D. Dynamics of OH Formation from CH_3ONO. It is well-known that alkyl nitrites occur as *cis* and *trans* (*syn* and *anti*) conformers in the gas phase at around room temperature. Intramolecular hydrogen bonds are widely present in the *cis* conformers, which generally make these conformers more stable.[47−52] In the case of the simplest alkyl nitrite, CH_3ONO, Günthard and co-workers[50,51,53] investigated the stabilization of both the *cis* and *trans* conformers using microwave and matrix IR experimental techniques. Felder and Günthard[53] found the *cis* conformer to be stabilized by 0.63 kcal/mol with respect to the *trans* conformer due to the intramolecular hydrogen bonds between the terminal oxygen atom and the methyl hydrogen atoms. Here, we proposed a reasonable photodissociation mechanism for the OH product pathway for methyl nitrite. After absorbing a 266 nm photon, the CH_3ONO molecule is excited to the S_2 state. The excited CH_3ONO molecule then relaxes to the S_0 or S_1 states through internal conversion. This is followed by intramolecular hydrogen atom transfer from the methyl group to the nitrite group via a five-membered-ring transition state. Subsequent N−OH bond cleavage releases the OH fragment in the S_0 or S_1 states. As an aid to understanding the proposed dissociation mechanism outlined above, we carried out DFT calculations on the PES of CH_3ONO corresponding to the OH photoproduct channel in the ground electronic state with the GAUSSIAN 03 program[54] at the B3LYP/6-311+G(d, p) level.

Figure 4 displays the relative energies after zero-point energy corrections and the optimized geometries of methyl nitrite, the intramolecular hydrogen atom transfer isomer, the transition state (TS), and the products. As shown in Figure 4, the parent molecule CH_3ONO first isomerizes to CH_2ONOH via a five-membered-ring transition state with a barrier of 58.70 kcal/mol and then dissociates to H_2CON + OH by breakage of the N−OH bond (72.36 kcal/mol). On the other hand, the intermediate CH_2ONOH can generate the HONO photoproduct through cleavage of the C−O bond (Figure 4). Once the nascent HONO product has an internal energy in excess of 48 kcal/mol, it decomposes into HO + NO.[55] Under the present experimental conditions, the internal energy (E_0) of the *trans* conformer of CH_3ONO has been evaluated as about 2.14 kcal/mol.[27] The internal energy (E_0) of the *cis* conformer of CH_3ONO is 0.63 kcal/mol lower than that of the *trans* conformer at $E_0 = 1.51$ kcal/mol. The energy of one 266 nm photon ($h\nu$) is 107.49 kcal/mol. An energy of 97.51 kcal/mol (D_0) is needed to generate the HONO photoproduct by breaking the C−O bond (Figure 4). Thus, the available energy corresponding to the HONO fragment channel (Figure 4) from the 266 nm photolysis of CH_3ONO is $E_{avl} = h\nu + E_0(CH_3ONO) - D_0(CH_2{-}ONOH) \approx 11.49$ kcal/mol, which is lower than 48 kcal/mol. Thus, this available energy is not enough to allow the HONO photoproduct to further dissociate into OH + NO. For the OH product pathway depicted in Figure 4, the energy barrier is 72.36 kcal/mol, which is 25.15 kcal/mol lower than that for the HONO product pathway. Therefore, it is much easier to produce OH than to produce HONO when CH_3ONO is photolyzed.

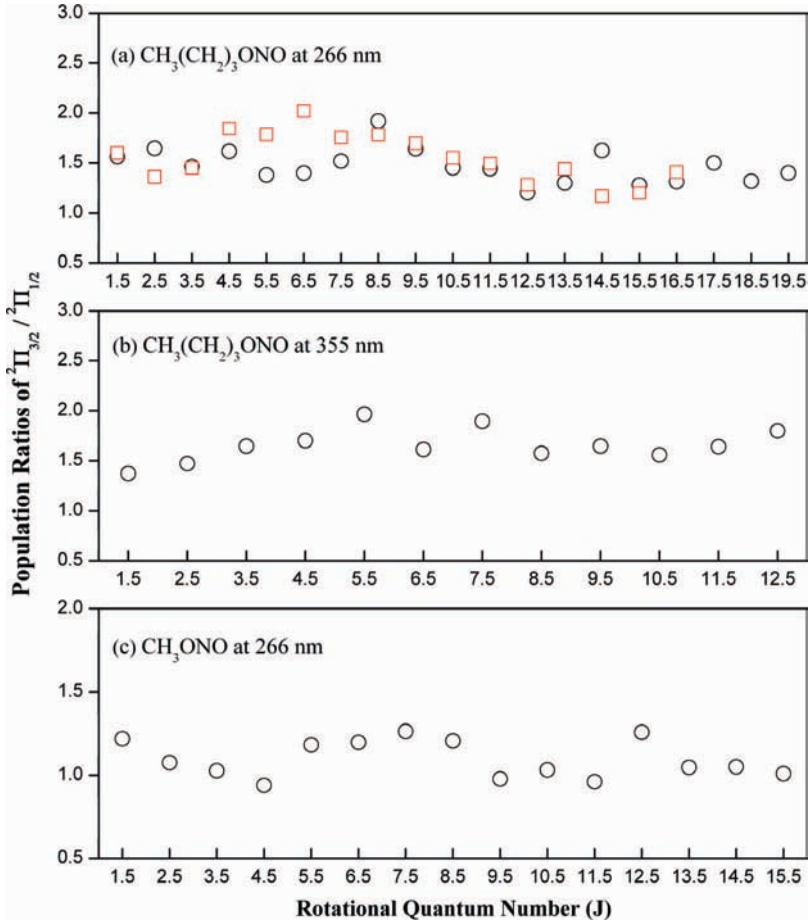

Figure 3. Spin−orbit population ratios of $^2\Pi_{3/2}/^2\Pi_{1/2}$ of the nascent OH from the photolysis of (a) $CH_3(CH_2)_3ONO$ at 266 nm, (b) $CH_3(CH_2)_3ONO$ at 355 nm, and (c) CH_3ONO at 266 nm. The open circles denote the OH vibrational ground state ($v'' = 0$); the open rectangles denote the OH vibrational excited state ($v'' = 1$).

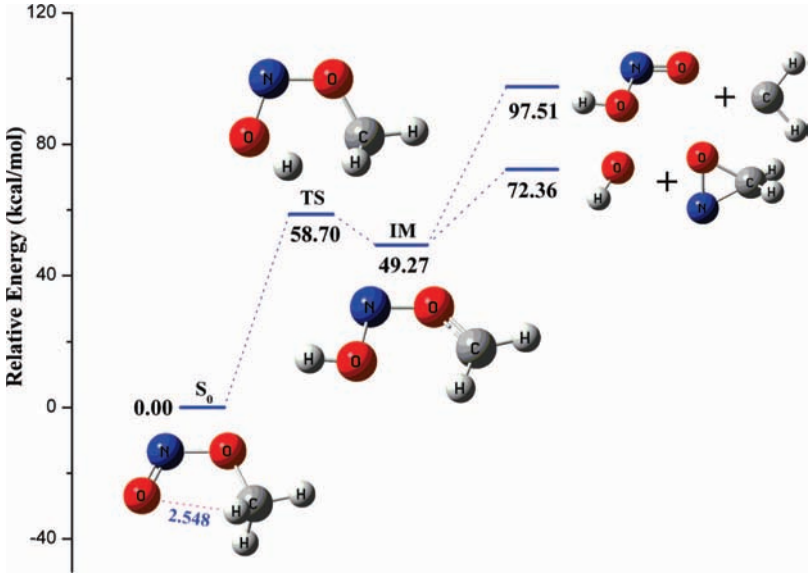

Figure 4. Schematic energy diagram for the hydrogen atom transfer and dissociation reaction of CH_3ONO calculated at the B3LYP/6-311+G(d,p) level. Energy units are in kcal/mol.

Another possible decay channel for the OH product through reactions according to eqs 2 and 3 was suggested in our previous Letter.[39] In the reaction according to eq 2, the dissociation energy of the CH_3O-NO bond is 41.46 kcal/mol.[27] The available energy for this reaction is $E_{avl} = h\upsilon + E_0(CH_3ONO) - D_0(CH_3O-NO) \approx 67.54$ kcal/mol. In the reaction according to eq 3, the methoxy radical, $CH_3O(X,^2E)$, needs an internal energy in excess of 89.71 kcal/mol to further dissociate into $CH_2 + OH$.[56] Therefore, it is more difficult to produce an OH fragment through this decay channel than through the OH product channel depicted in Figure 4.

As a test of the technique, we measured the rotational and vibrational state distributions of the nascent OH fragments derived from photolyses of HONO at 266 and 355 nm. The OH fragments

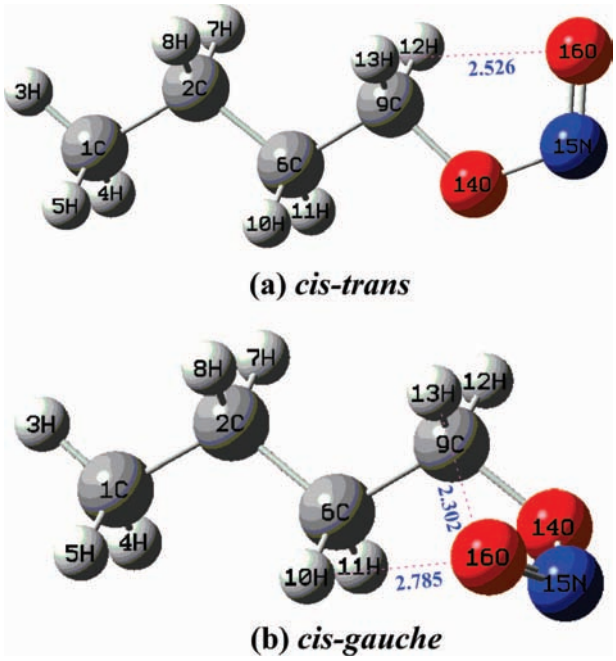

Figure 5. Equilibrium geometries of (a) the *cis-trans* and (b) the *cis-gauche* conformers of $CH_3(CH_2)_3ONO$, optimized at the B3LYP/6-311+G(d,p) level. Distances are given in Å.

produced by photodissociation of HONO at both wavelengths were found to be vibrationally cold. This was consistent with the results obtained by Kenner et al.[57] from the 193 nm photolysis of HONO and by Vasudev et al.[43] from 355, 369, and 342 nm photolyses of HONO. In the 355 nm photolysis of HONO studied in the present work, the rotational state distribution conformed to Boltzmann behavior with $T_{rot} = 342 \pm 50$ K, which was in good agreement with the result of $T_{rot} = 364 \pm 20$ K obtained by Vasudev et al.[43] at this wavelength. This indicated that our LIF experimental apparatus was adequate for studying the internal state distributions of the nascent photoproducts. In the 266 nm photodissociation of HONO, the rotational state distribution conformed to Boltzmann behavior and was well characterized by a rotational temperature of $T_{rot} = 742 \pm 50$ K. The rotational temperature ($T_{rot} = 2200 \pm 150$ K) of the OH from the photolysis of CH_3ONO at 266 nm was clearly much higher than that ($T_{rot} = 742 \pm 50$ K) of the OH from the photolysis of HONO at 266 nm. With regard to the respective OH product pathways, in contrast to the direct photolysis mechanism of HONO,[58] the above results may suggest that the photolysis of CH_3ONO is an indirect process, This would be consistent with the finding from our DFT calculations that CH_3ONO needs to traverse a transition state with a barrier of 58.70 kcal/mol to generate the OH photoproduct.

E. Dynamics of OH Formation from $CH_3(CH_2)_3ONO$. Four different equilibrium geometries (*cis-trans*, *cis-gauche*, *trans-gauche*, and *trans-trans*) of the ground electronic state of $CH_3(CH_2)_3ONO$ were determined in a very recent study by McLaughlin et al.[59] They found the *cis-trans* (*cis* with respect to the C—O—N═O dihedral angle and *trans* with respect to the C—C—O—N dihedral angle) and *cis-gauche* geometries to be the two most stable conformers due to their propensity for hydrogen bond formation between the nitrite group and the hydrogen atom on the α-carbon atom.[59] In the present work, we have optimized these two geometries using the GAUSSIAN 03 program[54] at the B3LYP/6-311+G(d, p) level. Panels a and b of Figure 5 display the *cis-trans* and *cis-gauche* conformers, respectively. As shown in Figure 5a, the distance between the terminal oxygen atom O(16) and the hydrogen atom H(13) on the α-carbon is 2.526 Å in the *cis-trans* conformer, which closely resembles the distance (2.548 Å) between the terminal oxygen atom and a methyl hydrogen atom in the CH_3ONO molecule (Figure 4). Therefore, the hydrogen bond strength between the nitrite group and the hydrogen atom on the α-carbon in $CH_3(CH_2)_3ONO$ is close to that in CH_3ONO. Similar to the photolysis mechanism for CH_3ONO mentioned above, a photodissociation mechanism of the *cis-trans* conformer of $CH_3(CH_2)_3ONO$ may be proposed for the OH product channel. After absorbing a 266 or 355 nm photon, the parent molecule $CH_3(CH_2)_3ONO$ is promoted to the S_2 or S_1 excited state. The excited $CH_3(CH_2)_3ONO$ molecule then relaxes to the S_0 or S_1 states through internal conversion. This is followed by intramolecular hydrogen atom transfer of the hydrogen atom H(13) from the α-carbon to the terminal oxygen atom O(16) via a five-membered-ring transition state. Subsequent N—OH bond cleavage releases the OH fragment.

As shown in Figure 5b, the distance between the terminal oxygen atom O(16) and the hydrogen atom H(13) on the α-carbon is 2.302 Å in the *cis-gauche* conformer, which is 0.224 Å shorter than that in the *cis-trans* conformer, thus indicating a stronger hydrogen bond. The distance between the terminal oxygen atom O(16) and the hydrogen atom H(10) on the *β*-carbon is 2.785 Å in the *cis-gauche* conformer, which is 0.259 Å longer than that in the *cis-trans* conformer. This suggests that a pseudo-hydrogen bond is formed between the terminal oxygen atom O(16) and the hydrogen atom H(10) on the *β*-carbon. Thus, a photodissociation mechanism may be proposed for the OH product pathway in the case of the *cis-gauche* conformer. After absorbing a 266 or 355 nm photon, the parent molecule $CH_3(CH_2)_3ONO$ is excited to the S_2 or S_1 state. The excited $CH_3(CH_2)_3ONO$ molecule then relaxes to the S_0 or S_1 states through internal conversion. This is followed by the intramolecular hydrogen atom transfer of the hydrogen atom from the α-carbon to the nitrite group via a five-membered-ring transition state and of the hydrogen atom from the *β*-carbon to the nitrite group via a six-membered-ring transition state. Subsequent N—OH bond cleavage releases the OH fragment.

According to the photodissociation mechanisms proposed above, three dissociation channels for the OH fragments are involved in the photolysis of *n*-butyl nitrite: the first one stems from photolysis of the *cis-trans* conformer via a five-membered-ring transition state, the second one stems from photolysis of the *cis-gauche* conformer via a five-membered-ring transition state, and the last one stems from photolysis of the *cis-gauche* conformer via a six-membered-ring transition state. Generally, a fast dissociation process readily leads to a non-Boltzmann rotational state distribution. In the experiments described herein, we detected the total OH product from the photolysis of *n*-butyl nitrite. The three OH product channels could not be discriminated, which would have led to complicated internal state distributions of the OH from the photolysis of *n*-butyl nitrite. This was in good agreement with the experimental findings: non-Boltzmann rotational state distributions of the OH $v'' = 0$ state from the photolyses of *n*-butyl nitrite at 355 and 266 nm; Boltzmann rotational state distribution of the OH $v'' = 1$ state from the photolysis of *n*-butyl nitrite at 266 nm; and a vibrational excited state distribution of the OH fragment from the photolysis of *n*-butyl nitrite at 266 nm. It can be inferred from the above photolysis mechanisms that the most likely channel for vibrationally excited OH formation is photolysis of the *cis-gauche* conformer via a six-membered-ring transition state.

IV. Conclusion

Using the one-photon LIF technique, we first observed the OH fragments from photolyses of gaseous CH_3ONO and

$CH_3(CH_2)_3ONO$ at 266 and 355 nm at room temperature. Detailed internal state distributions of the nascent OH fragments from the photolyses were measured. The OH fragment from the 266 nm photolysis of CH_3ONO was found to be vibrationally cold and its rotational state distribution conformed to Boltzmann behavior with a rotational temperature of T_{rot}=2200 ± 150 K. The OH fragment from the 355 nm photolysis of $CH_3(CH_2)_3ONO$ was also found to be vibrationally cold, but its rotational state distribution showed non-Boltzmann behavior. In the photodissociation of $CH_3(CH_2)_3ONO$ at 266 nm, the OH fragment was found to be vibrationally excited, and the measured relative population of $v'' = 0$:1 was 0.78:0.22. The rotational state distribution of the OH $v'' = 0$ state did not conform to a non-Boltzmann distribution, but the rotational state distribution of the $v'' = 1$ state did conform to Boltzmann behavior, with a rotational temperature of T_{rot}=1462 ± 120 K. Preferential population of the $^2\Pi_{3/2}$ spin−orbit state was observed for each vibrational state of the OH from all of the above photodissociations. Photolysis mechanisms involving hydrogen atom transfer processes have been proposed for the OH product pathway in the case of CH_3ONO and $CH_3(CH_2)_3ONO$. DFT calculations corresponding to the proposed mechanism have been carried out for the CH_3ONO molecule, the results of which were consistent with the experimental results. It is hoped that the findings of this study, especially those concerning photolysis pathway and mechanisms, may be utilized to predict the behavior of other alkyl nitrite molecules ($C_nH_{2n+1}ONO$, $n \geq 1$).

Acknowledgment. This work was supported by NKBRSF (2007CB815202), NSFC (20721004 and 20833008) and the knowledge innovation program of the Chinese Academy of Sciences (DICP R200603).

References and Notes

(1) Butler, L. J.; Neumark, D. M. *J. Phys. Chem.* **1996**, *100*, 12801.
(2) Huber, J. R.; Schinke, R. *J. Phys. Chem.* **1993**, *97*, 3463.
(3) (a) Schinke, R. *Photodissociation Dynamics*; Cambridge University Press: Cambridge, UK, 1993. (b) Han, K. L.; He, G. Z. *J. Photochem. Photobiol. C: Photochem. Rev.* **2007**, *8*, 56.
(4) Finke, H.; Spiecker, H.; Andresen, P. *J. Chem. Phys.* **1999**, *110*, 4777.
(5) Farmanara, P.; Stert, V.; Radloff, W. *Chem. Phys. Lett.* **1999**, *303*, 521.
(6) Ihm, H.; Scheer, K.; Celio, H.; White, J. M. *Langmuir* **2001**, *17*, 786.
(7) Lahmani, F.; Lardeux, C.; Solgadi, D. *Chem. Phys. Lett.* **1983**, *102*, 523.
(8) D'azy, O. B.; Lahmani, F.; Lardeux, C.; Solgadi, D. *Chem. Phys.* **1985**, *94*, 247.
(9) Lahmani, F.; Lardeux, C.; Solgadi, D. *Chem. Phys. Lett.* **1986**, *129*, 24.
(10) Hippler, M.; Al-Janabi, F. A. H.; Pfab, J. *Chem. Phys. Lett.* **1992**, *192*, 173.
(11) Hippler, M.; McCoustra, M. R. S.; Pfab, J. *Chem. Phys. Lett.* **1992**, *198*, 168.
(12) McCoustra, M. R. S.; Hippler, M.; Pfab, J. *Chem. Phys. Lett.* **1992**, *200*, 451.
(13) Keller, B. A.; Felder, P.; Huber, J. R *Chem. Phys. Lett.* **1986**, *124*, 135.
(14) Brühlmann, U.; Dubs, M.; Huber, J. R. *J. Chem. Phys.* **1987**, *86*, 1249.
(15) Suter, H. U.; Brühlmann, U.; Huber, J. R. *Chem. Phys. Lett.* **1990**, *171*, 63.
(16) Kades, E.; Rösslein, M.; Brühlmann, U.; Huber, J. R. *J. Phys. Chem.* **1993**, *97*, 989.
(17) Nonella, M.; Huber, J. R. *Chem. Phys. Lett.* **1986**, *131*, 376.
(18) Hennig, S.; Engel, V.; Schinke, R.; Nonella, M.; Huber, J. R. *J. Chem. Phys.* **1987**, *87*, 3522.
(19) Schinke, R.; Henning, S.; Untch, A.; Nonella, M.; Huber, J. R. *J. Chem. Phys.* **1989**, *91*, 2016.
(20) Nonella, M.; Huber, J. R.; Untch, A.; Schinke, R. *J. Chem. Phys.* **1989**, *91*, 194.
(21) Lahmani, F.; Lardeux, C.; Lavollée, M.; Solgadi, D. *J. Chem. Phys.* **1980**, *73*, 1187.
(22) Inoue, G.; Kawasaki, M.; Sato, H.; Kikuchi, T.; Kobayashi, S.; Arikawa, T. *J. Chem. Phys.* **1987**, *87*, 5722.
(23) Hippler, M.; McCoustra, M. R. S.; Pfab, J. *Chem. Phys. Lett.* **1992**, *198*, 168.
(24) Wang, X.; Wang, Y.; Lv, C.; Kubo, M.; Miyamoto, A. *J. Photochem. Photobio. A: Chem.* **2007**, *187*, 119.
(25) Winniczek, J. W.; Dubs, R. L.; Appling, J. R.; McKoy, V.; White, M. G. *J. Chem. Phys.* **1989**, *90*, 949.
(26) Yin, H.-M.; Sun, J.-L.; Li, Y.-M.; Han, K.-L.; He, G.-Z.; Cong, S.-L. *J. Chem. Phys.* **2003**, *118*, 8248.
(27) Keller, B. A.; Felder, P.; Huber, J. R. *J. Phys. Chem.* **1987**, *91*, 1114.
(28) Ebata, T.; Yanagishita, H.; Obi, K.; Tanaka, I. *Chem. Phys.* **1982**, *69*, 27.
(29) Mestdagh, J. M.; Berdah, M.; Dimicoli, I.; Mons, M.; Meynadier, P.; d'Oliveira, P.; Piuzzi, F.; Visticot, J. P.; Jouvet, C.; Lardeux-Dedonder, C.; Martrenchard-Barra, S.; Soep, B.; Solgadi, D. *J. Chem. Phys.* **1995**, *103*, 1013.
(30) Effenhauser, C. S.; Felder, P.; Huber, J. R. *J. Phys. Chem.* **1990**, *94*, 296.
(31) Tuck, F. *J. Chem. Soc., Faraday Trans. II* **1977**, *73*, 689.
(32) Lavi, R.; Schwartz-Lavi, D.; Bar, I.; Rosenwaks, S. *J. Phys. Chem.* **1987**, *91*, 5398.
(33) Schwartz-Lavi, D.; Rosenwaks, S. *J. Chem. Phys.* **1988**, *88*, 6922.
(34) Castle, K. J.; Abbott, J.; Peng, X.; Kong, W. *Chem. Phys. Lett.* **2000**, *318*, 565.
(35) Kades, E.; Rösslein, M.; Huber, J. R. *J. Phys. Chem.* **1994**, *98*, 13556.
(36) Schwartz-Lavi, D.; Bar, I.; Rosenwaks, S. *Chem. Phys. Lett.* **1986**, *128*, 123.
(37) Castle, K. J.; Kong, W. *J. Chem. Phys.* **2000**, *112*, 10156.
(38) Yue, X.-F.; Sun, J.-L.; Liu, Z.-F.; Wei, Q.; Han, K.-L. *Chem. Phys. Lett.* **2006**, *426*, 57.
(39) Inoue, G.; Akimoto, H.; Okuda, M. *J. Chem. Phys.* **1980**, *72*, 1769.
(40) Herzberg, G. *Molecular Spectra and Molecular Structure. I. Spectra of Diatomic Molecules*; Van Nostrand: New York, 1953.
(41) Luque, J.; Crosley, D. R. *J. Chem. Phys.* **1998**, *109*, 439.
(42) Kovacs, I. *Rotational Structure in the Spectra of Diatomic Molecule*; Adam Hilger Ltd.: London, UK, 1969.
(43) Vasudev, R.; Zare, R. N.; Dixon, R. N *J. Chem. Phys.* **1984**, *80*, 4863,.
(44) Lee, K. W.; Lee, K.-S.; Jung, K.-H.; Volpp, H.-R. *J. Chem. Phys.* **2002**, *117*, 9266.
(45) Yoon, M.-C.; Choi, Y. S.; Kim, S. K. *J. Chem. Phys.* **1999**, *110*, 11850.
(46) Upadhyaya, H. P.; Kumar, A.; Naik, P. D. *J. Chem. Phys.* **2003**, *118*, 2590.
(47) Cordell, F. R.; Boggs, J. E.; Skanche, A. *J. Mol. Struct.* **1980**, *64*, 57.
(48) Suter, H. U.; Nonella, M. *J. Phys. Chem. A* **1997**, *101*, 5580.
(49) Tarte, P. *J. Chem. Phys.* **1952**, *20*, 1570.
(50) Ghosh, P. N.; Bauder, A.; Günthard, H. H. *Chem. Phys.* **1980**, *53*, 39.
(51) Felder, P.; Ha, T. K.; Dwivedi, A. M.; Günthard, H. H. *Spectrochim. Acta* **1981**, *37A*, 337.
(52) Piette, L. H.; Ray, J. D.; Ogg, R. A. *J. Chem. Phys.* **1957**, *26*, 1341.
(53) Felder, P.; Günthard, H. H. *Chem. Phys.* **1982**, *71*, 9.
(54) Frisch, M. J. et al. *Gaussian 03, Revision C.02*; Gaussian, Inc.: Wallingford, CT, 2004.
(55) Radhakrishnan, G.; Parr, T.; Wittig, C. *Chem. Phys. Lett.* **1984**, *111*, 25.
(56) Cui, Q.; Moroluma, K. *Chem. Phys. Lett.* **1996**, *263*, 54.
(57) Kenner, R. D.; Rohrer, F.; Stuhl, F. *J. Phys. Chem.* **1986**, *90*, 2635.
(58) Yu, S. Y.; Zhang, C. G.; Huang, M. B. *Chem. Phys. Lett.* **2007**, *440*, 187.
(59) McLaughlin, R. P.; Donald, W. A.; Jitjai, D.; Zhang, Y. *Spectrochim. Acta* **2007**, *67A*, 178.

JP810731D